

# Two-Cell Power Allocation for Downlink CDMA\*

Chi Zhou<sup>†</sup>    Peifang Zhang<sup>‡</sup>    Michael L. Honig<sup>§</sup>    Scott Jordan<sup>¶</sup>

## Abstract

Power and code allocation across two adjacent cells is studied for the downlink of a Code-Division Multiple-Access (CDMA) voice network. Each user has a utility function that measures the user's willingness to pay, or *utility*, as a function of the received Signal-to-Interference-plus-Noise-Ratio (SINR). The objective is to maximize the total utility over the two cells subject to code and power constraints. When all active users receive the same utility, the optimal allocation is characterized by a pair of threshold radii for the two cells, where each radius specifies the set of active users in that cell. The behavior of the optimal radii are characterized as a function of load and available resources (power and codes). The corresponding optimal power allocation can be achieved through a pricing scheme, in which each base station announces a price for each resource, and each user responds by requesting the amount of resources that maximizes the user's surplus (utility minus cost). We show that, depending on the load and resource constraints, the two cells may have to coordinate, or exchange information, in order to maximize the total utility.

---

\*Manuscript submitted to *IEEE Transactions on Wireless Communications*, November 2002. This work was supported by the Northwestern-Motorola Center for Communications, by NSF under grant CCR-9903055, and by DARPA under grant N66001-00-1-8935. This paper was presented in part at *IEEE VTC 2001*, Atlantic City.

<sup>†</sup>Telecommunication and Information Technology Institute, Florida International University, Miami, FL 33174; e-mail: zhouc@fiu.edu.

<sup>‡</sup>Department of ECE, University of California, Irvine, 544D Engg. Tower, Irvine, CA 92697; e-mail: pfzhang@uci.edu.

<sup>§</sup>Department of ECE, Northwestern University, Evanston, IL 60208; e-mail: mh@ece.northwestern.edu.

<sup>¶</sup>Department of ECE, University of California, Irvine, 544D Engg. Tower, Irvine, CA 92697; e-mail: sjordan@uci.edu.

# 1 Introduction

Efficient allocation of resources in a wireless network must take into account user requests for Quality of Service (QoS) along with channel variations, and received interference across users. In addition, when resources are scarce, allocations should be weighted by relative priorities, or differences in the value of the service to each user. The latter objective has motivated the utility-based approach to power control presented in [5–7, 9–12]. Earlier related work on wireline resource allocation based on utilities and pricing is presented in [1–4].

In this paper, we study resource allocation for the downlink of a Code-Division Multiple Access (CDMA) voice network. As in prior work on utility-based resource allocation, we assume that each user has a utility function that specifies the utility the user derives from the service as a function of the received QoS, which is taken to be Signal-to-Interference-plus-Noise-Ratio (SINR). Our objective is to allocate resources, namely, power and codes, to maximize the total utility summed over all users, subject to constraints on the number of available codes and total transmit power in each cell. In contrast with prior work on utility-based power control and related pricing methods (e.g., [5–7, 9–13]), here we consider resource allocation over two adjacent (interfering) cells.

For the voice service considered, the utility as a function of SINR is modeled as a step function starting at zero utility. For purposes of analysis, we consider the case where the SINR at the step transition, and the height of the step are the same for all users. Each active user receives one code, corresponding to a fixed rate. Maximizing total utility is then equivalent to maximizing the number of active users. We characterize the optimal power and code allocation for a one-dimensional cellular model, previously considered in [12] for a single cell, in which there is a continuous uniform distribution of users along the line in each cell. (The loads, or user densities in the two cells can differ.) We explicitly account for other-cell interference by treating the codes in other cells as random, and assuming a matched filter receiver. The codes within each cell are assumed to be orthogonal, and we assume ideal channels (no multipath) with only distance-based attenuation.

The optimal power allocation is specified by the set of threshold radii of active users for the two cells. For a given cell, all users within the radius are active, and all users outside the radius are inactive. The set of feasible threshold radii determine a region, the shape of which depends on

the constraints on codes and power, in addition to model parameters, such as load, noise level, and attenuation vs. distance. We partition the space of feasible regions into different classes, which correspond to different shapes. For example, when the total available power is small, the region is convex, whereas when the total available power is large enough, the region is non-convex. In the latter case, the optimal allocation typically exhausts the available power in only one cell. The power consumed by the other cell is then limited by the amount of interference it generates. Although our analysis considers only the case where the utilities are the same across users, numerical examples are presented, which illustrate optimal power and code allocations when different users may receive different utilities.

We introduce a pricing scheme to distribute the resource allocation process, analogous to that proposed in [4] for resource allocation in a wireline network. Within each cell, the base station announces to the users a price per code and a price per unit transmitted power, and each user responds by requesting the amount of resources that maximizes the user's *surplus* (utility minus cost). Without coordination between the two cells, the corresponding fixed point may not be the global optimum. Hence in general, the two cells must exchange information to achieve the maximum total utility.

The rest of the paper is organized as follows. In Section 2, we present the user and network models. In Section 3, we formulate the power allocation problem for utility maximization, and in Section 4, we partition the space of feasible regions for the set of threshold radii into different classes. In Section 5, we characterize the optimal power allocation, and in Section 6, we present a pricing scheme which can achieve this allocation.

## 2 System Model

The one-dimensional, two-cell model considered is illustrated in Figure 1. A user location is specified by the distance  $r$  from the closest base station where  $r \leq 1$ . To facilitate our analysis, we assume a large system in which the number of users in cell  $i$ , denoted as  $K_i$ , and the processing gain  $N$  go to infinity with fixed ratios  $K_i/N$  for  $i = 1, 2$ . The density of users along the line in each cell is assumed to be constant for  $r$  between  $d_0 \ll 1$  (a reference point in the far field of the transmitter

antenna) and 1. (We assume  $d_0 > 0$  to avoid singularities in the path loss function.) The load in cell  $i$  is denoted as  $L_i = K_i/M$ , where  $M$  is the number of codes in the system. In what follows, we will assume that  $M = N$ .

The transmitted power to a user in cell  $i$  at distance  $r$  from the base station is denoted as  $P_{T,i}(r)$ . We assume distance-based attenuation represented by a path loss function  $h(r)$ . The power received by a user at distance  $r$  from the base station is  $P_{R,i}(r) = h(r)P_{T,i}(r)$ . We assume that  $h(r)$  is differentiable and strictly decreasing. In practice, the channel attenuation is not necessarily an increasing function of distance due to random shadowing and multipath; however, we can view the parameter  $r$  as a “radio distance” from the base station (defined by the attenuation), rather than an actual physical distance.

The codes are assumed to be orthogonal within each cell, but correlated between cells (due to a frequency reuse factor of 1). We assume that the multipath is negligible, or is equalized [14], and that the receiver is a matched filter. The received SINR for a user at distance  $r$  is

$$\xi(r) = \frac{P_{R,i}(r)}{\sigma^2 + I(r)} \quad (1)$$

where  $\sigma^2$  is the background noise variance, assumed to be the same for all users, and  $I(r)$  is the received interference power at the output of the matched filter. We can write

$$I(r) = P_{tot,j}h(2-r) \quad (2)$$

where  $j \neq i$ , and  $P_{tot,i}$  is the average transmitted power per code in cell  $i$ , and is given by

$$P_{tot,i} = \frac{L_i}{1-d_0} \int_{d_0}^1 P_{T,i}(r) dr. \quad (3)$$

As  $r$  increases, both the attenuation of the desired signal and the interference increase, so that more transmitted power is required to achieve a target SINR. Finally, we remark that the results in this paper can be easily extended to the case where the cell radius can exceed one.

### 3 Problem Formulation

In this section, we formulate optimal resource allocation problems based on the notion of user utility. Namely, we assume that each user has a *utility function*  $u(\xi)$ , where  $\xi$  denotes the received

SINR [17]. For the voice service considered, we model  $u(\xi)$  as a step, as shown in Figure 2, rising from zero utility when  $\xi < \xi_0$  to a positive utility  $u_0 > 0$  when  $\xi > \xi_0$ . The target SINR  $\xi_0$  is assumed to be the same for all users. The height of the step indicates the call's priority level. More important calls are associated with higher values of  $u_0$ , i.e., the user is willing to pay more to gain admission to the system. For the analytical results in this paper,  $u_0$  is assumed to be identical for all users; in numerical results, we will consider the case where  $u_0$  has a uniform distribution across users.

Our objective is to allocate power and codes across the users in both cells to maximize the total utility, subject to code and power constraints in each cell. Specifically, denoting the utility received by a user in cell  $i$  at distance  $r$  as  $U_i(r)$ , the total utility per code in cell  $i$  is given by

$$U_{tot,i} = \frac{L_i}{1 - d_0} \int_{d_0}^1 U_i(r) dr. \quad (4)$$

For the voice system considered, each active user is assigned one code, just enough power to reach the target SINR  $\xi_0$ , and receives utility  $u_0$ . Each inactive user receives zero power and codes, and zero utility. The code allocation is therefore determined by the power allocation. Specifically, letting  $C_{tot,i}$  be the fraction of requested codes in cell  $i$ , we have

$$C_{tot,i} = \frac{L_i}{1 - d_0} \int_{d_0}^1 \chi_i(r) dr = \frac{L_i}{1 - d_0} \text{meas}\{r : P_{T,i}(r) > 0, \quad 0 \leq r \leq 1\} \quad (5)$$

where  $\chi_i(r) = 1$  if the user at radius  $r$  is active, and is zero otherwise, and  $\text{meas}\{\mathcal{A}\}$  denotes the measure of the set  $\mathcal{A}$ . The optimization problem therefore reduces to determining the optimal power allocations  $P_{T,i}(r)$ ,  $i = 1, 2$ .

We can now state the two-cell optimal utility maximization problem for power allocation as:

$$\mathbf{Problem P1:} \quad \max_{\{P_{T,1}(r), P_{T,2}(r)\}} U_{tot} = U_{tot,1} + U_{tot,2} \quad (6)$$

$$\text{subject to} \quad C_{tot,i} \leq 1 \quad i = 1, 2 \quad (7)$$

$$P_{tot,i} \leq \mathcal{P} \quad i = 1, 2 \quad (8)$$

$$P_{T,i}(r) \geq 0 \quad i = 1, 2, \quad d_0 \leq r \leq 1 \quad (9)$$

where (7) and (8) are the code and power constraints, respectively, and  $\mathcal{P}$  is the available power per code at each base station.

The assumptions of a step utility function, which is the same for all users, and distance-based attenuation allow us to state an equivalent, but simpler version of the preceding problem. Namely, suppose that  $P_{T,i}(r)$  is restricted to form a *radius* of active users in cell  $i$ , denoted as  $r_i$ . That is, users at distance  $d_0 \leq r \leq r_i$  are active, and users at distance  $r_i < r \leq 1$  are inactive. We will refer to this type of power allocation as a *threshold allocation*. The associated utility maximization problem for threshold radius allocations is:

$$\mathbf{Problem P2:} \quad \max_{\{r_1, r_2\}} U_{tot} = U_{tot,1} + U_{tot,2} \quad (10)$$

$$s.t. \quad C_{tot,i} \leq 1 \quad i = 1, 2 \quad (11)$$

$$P_{tot,i} \leq P \quad i = 1, 2 \quad (12)$$

$$d_0 \leq r_i \leq 1, \quad i = 1, 2 \quad (13)$$

**Theorem 1:** *The optimal threshold allocation, determined by solving Problem P2, is the solution to Problem P1.*

**Proof:** Assume that the optimal policy is not a threshold policy. Swapping the furthest active user with the closest inactive user in a cell does not change the number of active users, and hence the total utility, but lowers the total power. Hence this gives a feasible allocation. Continuing to swap active and inactive users in this fashion leads to a threshold allocation.  $\square$

For a threshold allocation, we have

$$C_{tot,i} = \frac{L_i(r_i - d_0)}{1 - d_0} \quad (14)$$

$$P_{tot,i} = \frac{L_i}{1 - d_0} \int_{d_0}^{r_i} P_{T,i}(r; P_{tot,j}) dr \quad (15)$$

$$U_{tot,i} = u_0 C_{tot,i} = \frac{u_0 L_i(r_i - d_0)}{1 - d_0} \quad (16)$$

where  $P_{T,i}(r; P_{tot,j})$  is the transmission power required to achieve the target SINR  $\xi_0$ , i.e.,

$$P_{T,i}(r; P_{tot,j}) = \frac{\xi_0[\sigma^2 + P_{tot,j}h(2 - r)]}{h(r)} \quad i \neq j. \quad (17)$$

We can compute

$$\frac{\partial r_i}{\partial P_{tot,i}} = \frac{(1 - d_0)h(r_i)}{L_i \xi_0[\sigma^2 + P_{tot,j}h(2 - r_i)]} > 0, \quad (18)$$

$$\frac{\partial r_i}{\partial P_{tot,j}} = \frac{-h(r_i)b(r_i)}{\sigma^2 + P_{tot,j}h(2 - r_i)} < 0, \quad i \neq j \quad (19)$$

where  $b(r_i) = \int_{d_0}^{r_i} \frac{h(2-r)}{h(r)} dr$ . That is,  $r_i$  increases monotonically with  $P_{tot,i}$ , and decreases with  $P_{tot,j}$ . In what follows, unless otherwise stated, we will restrict ourselves to the class of threshold allocations.

## 4 Feasible Region

Define the *feasible region*  $\mathcal{R}$  as the set of threshold radii  $(r_1, r_2)$  for which the SINR, code, and power constraints can be satisfied, i.e.,

$$\mathcal{R} = \{(r_1, r_2) : \exists P_{T,i}(r), \quad i = 1, 2, \text{ such that } \xi_i(r) \geq \xi^* \text{ for } 0 \leq r \leq r_i, \quad (20)$$

$$P_{tot,i} \leq \mathcal{P}, \quad C_{tot,i} \leq 1, \text{ and } d_0 \leq r_i \leq 1 \text{ for } i = 1, 2\} \quad (21)$$

Note that  $\mathcal{R}$  is a compact set. The shape of  $\mathcal{R}$  depends on the load, available power to noise ratio  $\mathcal{P}/\sigma^2$ , and the path loss function  $h(r)$ . In what follows, we denote the *boundary* of a closed set  $\mathcal{S}$  as  $\bar{\mathcal{S}}$ . In the remainder of this section we relate the shape of  $\bar{\mathcal{R}}$  to the code and power constraints.

### 4.1 Boundary Constraints

Each point in  $\bar{\mathcal{R}}$  corresponds to a set of binding constraints. Specifically, for a given point in  $\bar{\mathcal{R}}$ , we call cell  $i$  *code-limited (CL)* if the code constraint is binding, *power-limited (PL)* if the power constraint is binding, and *demand-limited (DL)* if the cell size constraint is binding, i.e.,  $r_i = 1$ . Finally, we call cell  $i$  *interference-limited (IL)* if both the code and power constraints are loose, but cell  $i$  cannot increase  $r_i$  without decreasing  $r_j$  to satisfy the SINR constraints. That is, the interference generated by cell  $i$  prevents it from activating more users, assuming that the number of active users in cell  $j$  is held constant.

Each point in  $\bar{\mathcal{R}}$  can be classified according to the binding constraints, e.g., a boundary point is (PL,IL) if cell 1 is PL and cell 2 is IL. Note that not all combinations are possible. For example, if cell  $i$  is IL, then cell  $j$  must be PL. Otherwise, it would be possible to increase  $r_i$ , at least incrementally, without decreasing  $r_j$  (i.e., by increasing the power in both cells).

Points in  $\bar{\mathcal{R}}$  for which  $r_1 < 1$  and  $r_2 < 1$  are in the *Pareto set* [17]. That is, there is no other allocation, which can increase  $r_i$  without decreasing  $r_j$ . We are interested in classifying the shape of the Pareto set, which depends on the associated set of binding constraints.

## 4.2 Classification of Feasible Regions

We can view  $\mathcal{R}$  as the intersection of the regions defined by each constraint. Specifically, let  $r_{c,i}$  be the threshold radius at which the code constraint becomes binding, i.e.,  $C_{tot,i} = \frac{L_i(r_{c,i} - d_0)}{(1 - d_0)} = 1$ . The *code/demand region* is given by

$$\mathcal{C} = \{(r_1, r_2) : d_0 \leq r_i \leq \min(r_{c,i}, 1), \quad i = 1, 2\} \quad (22)$$

That is,  $\mathcal{C}$  is a rectangle, which contains the points that satisfy the cell size and code constraints only. Similarly, we define the *power region* as

$$\mathcal{Q} = \{(r_1, r_2) : \exists P_{T,i}(r), \quad i = 1, 2, \text{ such that } \xi_i(r) \geq \xi^*, \text{ for } 0 \leq r \leq r_i, \quad P_{tot,i} \leq \mathcal{P}, \text{ for } i = 1, 2\} \quad (23)$$

and the *power curve* as the boundary of  $\mathcal{Q}$ , denoted as  $\bar{\mathcal{Q}}$ . For any point in  $\bar{\mathcal{Q}}$ , we have  $P_{tot,i} = \mathcal{P}$  for some  $i$ . The feasible region is then  $\mathcal{R} = \mathcal{C} \cap \mathcal{Q}$ , and the Pareto set is  $\bar{\mathcal{R}} \cap \bar{\mathcal{Q}}$ . That is, the Pareto set is the section in  $\bar{\mathcal{R}}$  for which at least one cell is PL.

We now partition the set of feasible regions into three subsets, or classes. The class  $\mathcal{T}_1$  contains all feasible regions for which  $\mathcal{R} = \mathcal{C}$ . That is,  $\mathcal{R}$  is a rectangle defined only by the code and cell size constraints, as shown in Figure 3. The Pareto set includes only the corner point,  $(\min(1, r_{c,1}), \min(1, r_{c,2}))$ , at which each cell is either DL or CL, denoted as D/CL. Note that  $\mathcal{R} \in \mathcal{T}_1$  if and only if the point  $(\min(1, r_{c,1}), \min(1, r_{c,2}))$  is feasible.

A feasible region is in the class  $\mathcal{T}_2$  if it is convex, and is not in  $\mathcal{T}_1$ . That is, there exists a boundary point at which at least one cell is PL. Examples of feasible regions in  $\mathcal{T}_2$  are shown in Figure 4. Although the example in Figure 4 (d) looks essentially the same as the one shown in Figure 4 (a), it has been added because the point at which the utility is maximized is not at the (PL,PL) (corner) point. (See the discussion in Section 5.1.) Finally, a feasible region is in the class  $\mathcal{T}_3$  if it is non-convex. Examples are shown in Figure 5. In Figures 4 and 5,  $r_{p,i}$  is the threshold

radius at which the power constraint becomes binding, i.e.  $P_{tot,i} = \mathcal{P}$ . This radius depends on both  $L_i$  and  $P_{tot,j}$ , and reaches its maximum value  $r_{p,i}^{max}$  when  $P_{tot,j} = 0$ , and its minimum value  $r_{p,i}^{min}$  when  $P_{tot,j} = \mathcal{P}$ . The middle point  $(r_{p,1}^{min}, r_{p,2}^{min})$  is therefore (PL,PL).

If  $\mathcal{R}$  is in  $\mathcal{T}_2$  or  $\mathcal{T}_3$ , then  $\mathcal{R} = \mathcal{C} \cap \mathcal{Q} \neq \mathcal{C}$ . Figure 4 (a) shows an  $\mathcal{R} \in \mathcal{T}_2$  for which  $\mathcal{R} = \mathcal{Q}$ . For  $\mathcal{R} \in \mathcal{T}_2$ ,  $\bar{\mathcal{Q}}$  is concave, whereas for  $\mathcal{R} \in \mathcal{T}_3$ ,  $\bar{\mathcal{Q}}$  is not concave.

**Theorem 2:** *The power curve  $\bar{\mathcal{Q}}$  consists of two differentiable segments intersecting at the (PL,PL) point,  $(r_1, r_2) = (r_{p,1}^{min}, r_{p,2}^{min})$ . At the (PL,PL) point, the difference between left- and right-handed derivatives is*

$$\left. \frac{dr_2}{dr_1} \right|_{PL-} - \left. \frac{dr_2}{dr_1} \right|_{PL+} = \epsilon > 0, \quad (24)$$

where  $\epsilon \rightarrow 0$  as  $\mathcal{P}/\sigma^2 \rightarrow \infty$ .

**Proof:** From (15) and (17) we can write  $r_i = f_i(P_{tot,1}, P_{tot,2})$ ,  $i = 1, 2$ , where for fixed  $P_{tot,j}$  and differentiable  $h(r)$ ,  $f_i$  is a differentiable function of  $P_{tot,m}$ ,  $m \neq j$ . Fixing  $P_{tot,2} = \mathcal{P}$ , and increasing  $P_{tot,1}$  from zero to  $\mathcal{P}$  therefore traces a differentiable curve in the  $(r_1, r_2)$  plane from  $(d_0, r_{p,2}^{max})$  to  $(r_{p,1}^{min}, r_{p,2}^{min})$ . Similarly, fixing  $P_{tot,1} = \mathcal{P}$ , and decreasing  $P_{tot,2}$  from  $\mathcal{P}$  to zero traces a differentiable curve from  $(r_{p,1}^{min}, r_{p,2}^{min})$  to  $(r_{p,1}^{max}, d_0)$ .

At the (PL,PL) point, the left- and right-handed derivatives are

$$\left. \frac{dr_2}{dr_1} \right|_{PL-} = \left. \frac{\partial f_2}{\partial P_{tot,1}} \frac{\partial P_{tot,1}}{\partial r_1} \right|_{P_{tot,1}=P_{tot,2}=\mathcal{P}} = -\frac{c_1 b(r_{p,2}^{min}) P_{T,1}(r_{p,1}^{min}; \mathcal{P})}{P_{T,2}(r_{p,2}^{min}; \mathcal{P})} \quad (25)$$

$$\left. \frac{dr_2}{dr_1} \right|_{PL+} = \left. \frac{\partial f_2}{\partial P_{tot,2}} \frac{\partial P_{tot,2}}{\partial r_1} \right|_{P_{tot,1}=P_{tot,2}=\mathcal{P}} = -\frac{P_{T,1}(r_{p,1}^{min}; \mathcal{P})}{c_2 b(r_{p,1}^{min}) P_{T,2}(r_{p,2}^{min}; \mathcal{P})}. \quad (26)$$

where  $c_i = \frac{L_i \xi_0}{(1-d_0)}$  and  $b(r_i)$  is defined after (19). Since  $\mathcal{P}/\sigma^2 = \frac{c_i a(r_{p,i}^{min})}{1 - c_i b(r_{p,i}^{min})}$ , where  $a(r_i) = \int_{d_0}^{r_i} \frac{1}{h(r)} dr$ , it follows that  $c_i b(r_{p,i}^{min}) \leq 1$ , and equality holds only for  $\mathcal{P}/\sigma^2 \rightarrow \infty$ . Therefore  $c_1 b(r_{p,2}^{min}) \leq c_1/c_2$  and  $1/[c_2 b(r_{p,1}^{min})] \geq c_1/c_2$ . Combining with (26) gives the theorem.  $\square$

For  $\mathcal{R} \in \mathcal{T}_2$ , the two segments of  $\bar{\mathcal{Q}}$  are concave, as shown in Figure 4. For  $\mathcal{R} \in \mathcal{T}_3$ , these segments may be partly concave and convex, as shown in Figures 5 (a) and (b), or convex, as shown in Figure 5 (c). The Pareto set,  $\bar{\mathcal{R}} \cap \bar{\mathcal{Q}}$ , is shown as the segment between points  $A$  and  $B$  in both Figures 4 and 5. At point  $A$ , cell 2 is either PL, or is both PL and D/CL (P+D/CL). Similarly, at point  $B$ , cell 1 is either PL or P+D/CL.

There is a unique point on the power curve at which both cells are PL, although this point may or may not be feasible. Points on the AB segment to left of the (PL,PL) point are (IL,PL), whereas points on the AB segment to the right of the (PL,PL) point are (PL,IL).

### 4.3 Variation with Power Supply

In this section, we study how  $\mathcal{R}$  changes with the power supply  $\mathcal{P}$ . We start with two examples. Figure 6 shows  $\bar{\mathcal{R}}$  with different values of  $\mathcal{P}$ . For the first example, shown in Figure 6(a), the loads  $L_1 = 0.6, L_2 = 0.9$ , the path loss function  $h(r) = (d_0/r)^2$ , and the SINR target  $\xi_0 = 15$  dB. The available power to noise ratio  $\mathcal{P}/\sigma^2$  ranges from 20 to 38 dB. As  $\mathcal{P}$  increases, we observe that  $\mathcal{R}$  transits from class  $\mathcal{T}_2$  (for the smallest two values of  $\mathcal{P}$ ) to  $\mathcal{T}_3$ . When  $\frac{\mathcal{P}}{\sigma^2} = 20$  and 23 dB, the power curve is concave and the (PL,PL) point is optimal, as in Figure 4(a). For  $\frac{\mathcal{P}}{\sigma^2} = 29$  dB,  $\bar{\mathcal{R}}$  is concave near the ends, and convex near the middle, as in Figure 5(a). When  $\frac{\mathcal{P}}{\sigma^2} = 32$  dB,  $\bar{\mathcal{R}}$  consists of the intersection of a similar power curve with the code-demand boundary, as in Figure 5(b). When  $\frac{\mathcal{P}}{\sigma^2} = 38$  dB, the intersection of the power curve with  $\mathcal{R}$  consists of two strictly convex segments which intersect at the (PL,PL) point, as in Figure 5(c).

For the second example, shown in Figure 6(b), the loads  $L_1 = 0.7, L_2 = 1.2$ , the path loss function  $h(r) = (d_0/r)^4$ , and the SINR target  $\xi_0 = 10$  dB. The value of  $\frac{\mathcal{P}}{\sigma^2}$  ranges from 30 to 48 dB. In this example,  $\mathcal{R}$  transits from class  $\mathcal{T}_2$  to  $\mathcal{T}_1$  when  $\frac{\mathcal{P}}{\sigma^2} = 48$  dB. In all cases, the intersection of the power curve with  $\bar{\mathcal{R}}$  is concave. In all cases except for the largest two values of  $\mathcal{P}$ , the (PL,PL) point is feasible, as in Figure 4(a). For  $\frac{\mathcal{P}}{\sigma^2} = 45$  the (PL,PL) point is above point A, as shown in Figure 4(b).

To explain the transitions shown in Figure 6, we note that as  $\mathcal{P} \rightarrow 0$ , both  $r_{p,i}^{max}$  and  $r_{p,i}^{min}$  approach  $d_0$ . As  $\mathcal{P} \rightarrow \infty$ ,  $r_{p,i}^{max} \rightarrow \infty$ , and  $r_{p,i}^{min}$  converges to a finite value, given by  $c_i b(r_{p,i}^{min}) = 1$ . This observation motivates the following two theorems, which state that as  $\mathcal{P}$  increases, the shape of the power curve segments change from concave to convex.

**Theorem 3:** *If  $h(r) = (d_0/r)^n$  for any  $n > 1$ , then there exists a power level  $P_L$  such that for  $P \leq P_L$ , the two power curve segments are concave, and therefore  $\mathcal{R}$  is a convex region.*

**Theorem 4:** *Suppose that  $\frac{h(r')}{h(2-r')} \int_{d_0}^{r'} \frac{h(2-r)}{h(r)} dr$  is an increasing function of  $r'$ . Then there exists*

a power level  $\mathcal{P}_H$  such that for  $\mathcal{P}_H \leq \mathcal{P} < \infty$ , the two power curve segments are convex.

The proofs are given in Appendix A.

Note that the condition that  $\frac{h(r')}{h(2-r')} \int_{d_0}^{r'} \frac{h(2-r)}{h(r)} dr$  is an increasing function of  $r'$  is satisfied by  $h(r) = 1/r^n$ ,  $n > 0$ .

The progression from concave to convex power curve segments corresponds to an increase in other-cell interference relative to the background noise. Namely, for small  $\mathcal{P}$ , the other-cell interference is relatively small, and the incremental decrease in  $r_2$  due to an incremental increase in  $r_1$  (caused by the associated incremental interference) decreases with  $r_1$ . In contrast, for large  $\mathcal{P}$ , the interference dominates the noise, and the incremental decrease in  $r_2$  due to an incremental increase in  $r_1$  is more severe for smaller  $r_1$ .

## 5 Optimal Resource Allocation

The results in the preceding section are now used to characterize the optimal resource allocation. We will compare coordinated optimization, where the cells coordinate to maximize total utility, with uncoordinated optimization, where each cell maximizes its own utility without regard to the effect on the other cell.

### 5.1 Coordinated Resource Allocation

For the case where all users receive the same utility and the channel gain is determined by distance-based attenuation, we have the following result.

**Theorem 5:** *The solution to P2 maximizes  $L_1 r_1 + L_2 r_2$ , the number of active users per code, and is in  $\bar{\mathcal{R}}$ .*

**Proof:** The first statement follows directly from the optimality of a threshold allocation, (6), and (16). Since  $L_1 r_1 + L_2 r_2$  increases with  $r_1$  and  $r_2$ , the solution must be on the boundary of  $\mathcal{R}$ .  $\square$

Contours of the objective  $L_1 r_1 + L_2 r_2$  in the  $(r_1, r_2)$  plane are lines with slope  $-L_1/L_2$ . Hence we seek the furthest such line from the origin, which intersects  $\mathcal{R}$ . Note that all intersection points must be in the Pareto set, since otherwise an allocation exists that increases the utility in one cell

without decreasing the utility in the other cell. For convex  $\mathcal{R}$ , *any* point in  $\bar{\mathcal{R}}$ , which is tangent to a line with slope  $-L_1/L_2$ , is optimal. In Figures 3, 4, and 5 optimal points are labelled with an asterisk. Note in particular, that the optimal points in Figures 4 (a) and (d) differ due to the different choices of loads in the two cells. In Figure 4 (d),  $L_2 \gg L_1$  so that at the optimal point cell one is IL.

In what follows, we let  $\bar{C}_i = \max(r_i, C_{tot,i})$ , and combine the cell size and code constraint into a single constraint  $\bar{C}_i \leq 1$ . Applying the Kuhn-Tucker theorem [16, Ch. 6] to Problem P2 gives the following set of necessary conditions for the optimal allocation,

$$\frac{\partial U_{tot}}{\partial r_i} - \lambda_{c,i} \frac{\partial \bar{C}_i}{\partial r_i} - \lambda_{p,i} \frac{\partial P_{tot,i}}{\partial r_i} - \lambda_{c,j} \frac{\partial \bar{C}_j}{\partial r_i} - \lambda_{p,j} \frac{\partial P_{tot,j}}{\partial r_i} = 0, \quad (i = 1, 2 \text{ and } i \neq j) \quad (27)$$

and

$$\lambda_{c,1}(1 - \bar{C}_1) + \lambda_{p,1}(\mathcal{P} - P_{tot,1}) + \lambda_{c,2}(1 - \bar{C}_2) + \lambda_{p,2}(\mathcal{P} - P_{tot,2}) = 0 \quad (28)$$

where  $(\lambda_{c,1}, \lambda_{c,2}, \lambda_{p,1}, \lambda_{p,2})$  is the set of nonnegative shadow costs for the code/radius and power constraints in each cell, and (28) is a complementary slackness condition that ensures each shadow cost is strictly positive iff the associated constraint is binding. In Appendix B, we give expressions for the shadow costs, which satisfy (27)-(28), in terms of  $(r_1, r_2)$ , the system parameters and path loss function.

If  $\mathcal{R}$  is convex (i.e., in  $\mathcal{T}_1$  or  $\mathcal{T}_2$ ), then the Kuhn-Tucker conditions specify a unique global optimum. This is because the objective function  $L_1 r_1 + L_2 r_2$  is linear, and therefore concave. If  $\mathcal{R} \in \mathcal{T}_3$ , then there may be more than one local optimum, i.e., more than one point in  $\bar{\mathcal{R}}$ , which is tangent to a line with slope  $-L_1/L_2$ . Empirical evidence suggests that there are typically a small set of local optima (c.f. Figure 5(a)-(c)). We have observed at most three such local optima, the (PL,PL) point, and one point each on the (IL,PL) and (PL,IL) segments. When  $L_1 < L_2$  we conjecture that the optimal point is either the (PL,PL) point or the local optimum on the (IL,PL) segment.

The shape of  $\bar{\mathcal{R}}$  changes continuously with  $\mathcal{P}$ ,  $L_1$ , and  $L_2$ . This is illustrated in Figure 6, where the optimal point on each power curve is marked with an asterisk. When  $\mathcal{P}$  is small, and  $\mathcal{R}$  is convex, the (PL,PL) point is optimal, and moves continuously with  $\mathcal{P}$ . In some cases, e.g.,

in Figure 6(a), at moderate values of  $\mathcal{P}$ , the power curve becomes a combination of concave and convex segments, and the optimal point may jump from the (PL,PL) point to a tangent point on the (IL,PL) segment. As  $\mathcal{P}$  continues to increase, the optimal point moves continuously with  $\mathcal{P}$ , following the tangent point.

(?)

## 5.2 Uncoordinated Resource Allocation

In this section, we assume that each cell maximizes its own utility, ignoring the effect this has on the other cell. Specifically, the optimization problem is for  $i = 1, 2$ ,

$$\textbf{Problem Unc:} \quad \max_{r_i} U_{tot,i} = \frac{u_0 L_i (r_i - d_0)}{1 - d_0} \quad (29)$$

$$s.t. \quad C_{tot,i} \leq 1 \quad (30)$$

$$P_{tot,i} \leq \mathcal{P} \quad (31)$$

where the SINR in cell  $i$  and  $U_{tot,i}$  both depend on  $P_{tot,j}$ , which results from the optimization in cell  $j$ . The corresponding equilibrium, in which cell  $i$  cannot increase its utility given fixed interference from cell  $j$  and vice versa, is called a *Nash equilibrium*.

**Theorem 6:** *At the Nash equilibrium, each cell is either DL, CL, or PL.*

**Proof:** This follows from the observation that the solution to Problem Unc is obtained by increasing  $r_i$  until one of the constraints is binding.  $\square$

Note, in particular, that a cell cannot be IL at the Nash equilibrium. That is, a cell  $i$  can always increase  $U_{tot,i}$  by increasing  $P_{tot,i}$ . Note also that if coordinated optimization gives cells which are any combination of D/CL and PL, then the optimal point is a Nash equilibrium.

We therefore conclude that if  $\mathcal{P}$ ,  $L_1$ , and  $L_2$  are chosen so that  $\mathcal{R} \in \mathcal{T}_1$ , then no coordination is needed between the cells to maximize the total utility. For  $\mathcal{R} \in \mathcal{T}_2$ , no coordination is needed unless one of the cells is IL at the optimal point, as illustrated in Figure 4 (d). For the latter case, and for  $\mathcal{R} \in \mathcal{T}_3$ , coordination is needed to reduce the power in the IL cell.

## 6 Resource Allocation via Pricing

In this section we present a distributed solution to Problem P2, motivated by the application of pricing to resource allocation. We first observe that for continuous, decreasing  $h(r)$ , any point  $\mathbf{r} \in \mathcal{R}$  corresponds to a unique point in the  $(P_{tot,1}, P_{tot,2})$  plane, and vice versa. Problem P2 is therefore equivalent to finding the point in the  $(P_{tot,1}, P_{tot,2})$  plane, which maximizes the total utility. The corresponding Lagrangian is given by

$$\mathcal{L} = \sum_{i=1}^2 (U_{tot,i} - \alpha_{p,i} P_{tot,i} - \alpha_{c,i} C_{tot,i}) \quad (32)$$

where the multipliers  $(\alpha_{p,i}, \alpha_{c,i})$ ,  $i = 1, 2$ , are chosen to satisfy the power constraints  $P_{tot,i} = P_{tot,i}^*$ ,  $i = 1, 2$ , where  $P_{tot,i}^*$  is the optimal power in cell  $i$ . Note that  $\alpha_{p,i}$  differs from the shadow cost  $\lambda_{p,i}$  in (27) since  $\lambda_{p,i} = 0$  if  $P_{tot,i}^* < \mathcal{P}$ , whereas  $\alpha_{p,i} > 0$  since it is selected to enforce the more restrictive power constraint (e.g., if the cell is IL). In contrast, the price per code  $\alpha_{c,i} = \lambda_{c,i}$ .

Substituting for  $U_{tot,i}$ ,  $P_{tot,i}$ , and  $C_{tot,i}$  in (32) from (4), (15), and (5), respectively, it follows that to maximize  $\mathcal{L}$  for a fixed  $(\alpha_{c,i}, \alpha_{p,i})$ , the user at radius  $r$  should choose the transmitted power  $P_i(r)$  to maximize  $U_i(r) - \alpha_{p,i} P_i(r) - \alpha_{c,i}$ . For the step utility function considered, this implies that the user at radius  $r$  is active iff the received utility  $u_0 \geq \alpha_{p,i} P_{T,i}(r) + \alpha_{c,i}$ , where  $P_{T,i}(r)$  is the transmitted power needed to achieve the target SINR. We therefore interpret  $\alpha_{p,i}$  and  $\alpha_{c,i}$  as *prices* for power and codes, respectively, in cell  $i$ .

A set of prices defines a threshold allocation, since  $P_{T,i}(r; P_{tot,j})$  increases with  $r$ . The threshold radius  $r_i$  satisfies

$$u_0 = \alpha_{p,i} P_{T,i}(r_i; P_{tot,j}) + \alpha_{c,i} \quad (33)$$

We can select prices to achieve any point in  $\mathcal{R}$ , since for any fixed  $(\alpha_{c,2}, \alpha_{p,2})$ ,  $r_1 = d_0$  can be achieved with any  $(\alpha_{c,1}, \alpha_{p,1})$  that satisfy  $u_0 < \alpha_{c,1} + \alpha_{p,1} P_{T,1}(d_0, P_{tot,2})$ , and  $r_1 = 1$  can be achieved by taking  $\alpha_{c,1} = \alpha_{p,1} = 0$ . Any  $d_0 < r_1 < 1$  is achievable since  $P_{T,1}(r; P_{tot,2})$  is a continuous, increasing function of  $r$ . The optimal set of prices is not unique in general. For example, when both cells are CL, there are an infinite number of price combinations, which give the optimal  $(r_1, r_2)$ .

We therefore conclude that the following pricing scheme can achieve the solution to Problem P2:

- The base station in cell  $i$  announces a price per code  $\alpha_{c,i}$  and a price per unit transmitted power  $\alpha_{p,i}$ .
- Each user responds by requesting the transmitted power  $P_{T,i}$ , which achieves the target SINR, provided that  $u_0 \geq \alpha_{p,i}P_{T,i}(r) + \alpha_{c,i}$ .

As previously observed, the two base stations may or may not need to coordinate in order to maximize the total utility. If the Nash equilibrium is optimal, then coordination is unnecessary, and each base station can independently adjust its prices to increase the utility within its cell until a resource is exhausted. If at the optimal allocation one of the cells is IL, then the corresponding base station must enforce the constraint  $P_{tot,i} < \mathcal{P}$  by charging a higher price for power than it would without coordination.

For the case where neither of the cells are D/CL at the optimal allocation, it is easily shown that  $\alpha_{p,i} = \frac{\partial U_{tot,i}}{\partial P_{tot,i}}$ . Furthermore, the shadow cost

$$\lambda_{p,i} = \frac{\partial U_{tot}}{\partial P_{tot,i}} = \alpha_{p,i} - \beta_{ji} \quad (34)$$

where  $\beta_{ji} = -\frac{\partial U_{tot,j}}{\partial P_{tot,i}}$  is the (nonnegative) *externality price* for power in cell  $i$ , which accounts for the interference to cell  $j$ . For the case where cell  $i$  is IL,  $\lambda_{p,i} = 0$ , hence the marginal increase in  $U_{tot,i}$  due to an increase in  $P_{tot,i}$  is equal to the corresponding marginal decrease in  $U_{tot,j}$ .

The externality prices  $\beta_{ji}$  and  $\beta_{ij}$  represent the information, which must be exchanged between the cells, to achieve the optimal allocation. Specifically, suppose that in Problem Unc, the objective is replaced by

$$U_{net,i} = U_{tot,i} - \beta_{ji}P_{tot,i} \quad (35)$$

In that case,  $\beta_{ji}$  can be chosen so that the shadow costs associated with the Kuhn-Tucker conditions match those for the coordinated problem. Specifically, to achieve radius  $r_i$ ,

$$\beta_{ji} = -\frac{\partial U_{tot,i}}{\partial P_{tot,j}} = \begin{cases} \frac{\xi_{0c_i}b(r_i)}{P_{T,i}(r_i, P_{tot,j})} \left(1 - \frac{\alpha_{c,i}}{u_0}\right), & \text{if cell } i \text{ is CL} \\ \frac{\xi_{0c_i}b(r_i)}{P_{T,i}(r_i, P_{tot,j})}, & \text{if cell } i \text{ is not CL} \end{cases} \quad (36)$$

Hence “uncoordinated” optimization of  $U_{net,i}$  in each cell, with appropriate externality prices, is equivalent to coordinated optimization.

## 6.1 Optimal Prices versus Load

In this section, we present a set of numerical examples, in which we fix the load  $L_1$  and vary  $L_2$ . In contrast to the preceding sections in which the utility per active user,  $u_0$ , was assumed to be identical for all users, we now assume that  $u_0$  is drawn from a uniform distribution on the interval 0 to 20, independently for each user. The optimal resource allocation can no longer be described by a set of threshold radii  $(r_1, r_2)$ , since at some distances only users with sufficiently high utility will be active. For this more general case, Kuhn-Tucker conditions again give shadow costs on power and codes within each cell, so that the pricing scheme in Section 6 can achieve the maximum utility.

The utility maximizing prices,  $(\alpha_{c,1}, \alpha_{p,1}, \alpha_{c,2}, \alpha_{p,2})$ , were found using a gradient search, and are plotted in Figure 7(a-b). In each pair of graphs,  $\frac{P}{\sigma^2} = 23$  dB, the SINR target  $\xi_0 = 5$  dB, and  $L_1$  is shown in the Figure caption. In addition to the prices, we also plot the shadow costs  $(\lambda_{c,1}, \lambda_{p,1}, \lambda_{c,2}, \lambda_{p,2})$ . As discussed in the preceding section,  $\alpha_{c,i} = \lambda_{c,i}$ , and  $\alpha_{p,i}$  is the sum of the shadow cost  $\lambda_{p,i}$  and the externality price  $\beta_{ji}$ .

In the first set of examples, shown in Figure 7(a),  $L_1 = 0.7$ . At low loads ( $0 \leq L_2 \leq 0.7$ ) all demand can be accommodated. Hence all prices are zero, and both cells are DL. At moderate loads ( $0.8 \leq L_2 \leq 1.1$ ) cell 2’s power constraint becomes binding, and the cells are (IL,PL). Correspondingly, the shadow cost on cell 2’s power constraint,  $\lambda_{p,2}$ , increases with load, along with the power prices  $\alpha_{p,1}$  and  $\alpha_{p,2}$ . The number of active users in each cell is now limited by other-cell interference, so that the externality prices increase.

At high loads,  $1.2 \leq L_2 \leq 2.0$ , cell 2’s code constraint becomes binding, and the cells are (IL,P+CL). Correspondingly, the shadow cost on cell 2’s code constraint,  $\lambda_{c,2}$ , increases with load, as does the price per code,  $\alpha_{c,2}$ . This charge for a code somewhat lessens the demand for power in both cells, and hence the power prices decrease in this load range.

In the second set of examples, shown in Figure 7(b), cell 1 is over-loaded ( $L_1 = 1.2$ ). At low loads in cell 2,  $0 \leq L_2 \leq 0.3$ , all demand can be accommodated in cell 2, but cell 1 has already

run out of codes. The cells are therefore (CL,DL), and  $\alpha_{c,1} = \lambda_{c,1} > 0$ . For  $0.4 \leq L_2 \leq 0.7$ , cell 1 exhausts its power supply; the cells are (C+PL,IL), and the externality and power prices are both positive. This reduces the demand for codes in cell 1, so that for  $0.8 \leq L_2 \leq 0.9$ , the code constraint in cell 1 is no longer binding, and the cells are (PL,IL). For  $1 \leq L_2 \leq 1.3$ , the code constraint in cell 2 is binding, and the cells are (PL,PL). Finally, for  $1.4 \leq L_2 \leq 2.0$ , the code constraint in cell 2 is also binding, and the cells become (PL,P+CL).

## 7 Conclusions

We have studied downlink code and power allocation across users in two adjacent CDMA cells. Our model accounts for the interference between the two cells. The performance objective is total utility summed over all users, where the utility function assigned to each user is a step function, corresponding to a fixed-rate (voice) service.

For the case where each user has the same utility function, the optimal resource allocation is specified by the set of threshold radii in each cell. We have characterized the shape of the feasible region, i.e., set of possible threshold radii, in terms of the resource constraints, target SINR, load, and path loss function. As the power constraint in each cell increases, we have shown that this region makes a transition from convex to non-convex. If this region is convex, and with equal loads in each cell, then both cells are resource limited at the optimal point. With unequal loads, it is possible for one cell to be interference-limited at the optimal point, i.e., it is restricted to a lower power than what is available in order to reduce the associated externality due to interference. When the feasible region is non-convex, one cell is typically interference-limited at the optimal point.

The optimal code and power allocation can be achieved with a pricing scheme. Namely, each base station announces a price per code and a price per unit transmitted power, and each user within the cell is active provided that the received utility exceeds the total charge for code and power. The resource allocation problem is then equivalent to finding the prices that maximize the total utility. If the two cells do not coordinate, or exchange information, then the corresponding Nash equilibrium may or may not be optimal, depending on the load and constraints. Specifically, if one cell is interference-limited at the optimal allocation, then the Nash equilibrium is not optimal.

In that case, the optimal allocation can be achieved by adding an externality charge to the power price.

The utility-based framework for resource allocation presented here can be applied to different traffic, utility, and system models. For example, related work on two-cell resource allocation for data traffic, and for voice traffic with multiple priorities is presented in [15,18]. Other propagation models, which account for random fading, could also be incorporated into the path loss function. Extending this analysis to a two-dimensional cellular model, or a one-dimensional multi-cell model with more than two cells appears to be difficult in general, although performance measures such as total utility can be studied numerically. We expect that for many cases of interest, results analogous to those presented here also apply to those more general models.

**Acknowledgment:** The authors thank Randall Berry for helpful discussions concerning this work.

## A Proofs of Theorems 3 and 4

Using (15) and (17), we can directly compute the following derivative at any point in the (IL,PL) segment of  $\bar{\mathcal{Q}}$ ,

$$\begin{aligned} \frac{d^2 r_2}{dr_1^2} = & - \frac{c_1 b(r_2) \xi_0}{P_{T,2}(r_2, P_{tot,1})} \left[ \frac{\sigma^2}{h(r_1)} \frac{|h'(r_1)|}{h(r_1)} + \mathcal{P} \frac{h(2-r_1)}{h(r_1)} \left( \frac{|h'(r_1)|}{h(r_1)} + \frac{|h'(2-r_1)|}{h(2-r_1)} \right) \right] \\ & - \frac{\xi_0 (c_1 b(r_2) P_{T,1}(r_1, \mathcal{P}))^2}{P_{T,2}(r_2, P_{tot,1})^3} \left[ \frac{\sigma^2}{h(r_2)} \frac{|h'(r_2)|}{h(r_2)} + P_{tot,1} \frac{h(2-r_2)}{h(r_2)} \left( \frac{|h'(r_2)|}{h(r_2)} + \frac{|h'(2-r_2)|}{h(2-r_2)} \right) \right] \\ & + \frac{2b(r_2)(c_1 P_{T,1}(r_1, \mathcal{P}))^2 h(2-r_2)}{P_{T,2}(r_2, P_{tot,1})^2 h(r_2)}, \end{aligned} \quad (37)$$

where  $h'(r) = dh(r)/dr$ . We have used the fact that  $P_{tot,2} = \mathcal{P}$  for any point in the (IL,PL) segment. As  $\mathcal{P} \rightarrow 0$ ,  $P_{tot,i}$ ,  $P_{T,i}(r_i, \mathcal{P})$ , and  $r_i$ ,  $i = 1, 2$ , all go to zero. Focusing on the terms in brackets, we first observe that for small enough  $\mathcal{P}$  and  $\sigma^2 > 0$ , we must have  $\sigma^2 \gg P_{tot,1} h(2-r_i)$  and  $\sigma^2 \gg \mathcal{P} h(2-r_i)$ . Also, since  $|h'(r)| > |h'(2-r)|$  for small  $r$ , we can ignore the right terms in the brackets.

As for the remaining terms,  $r_i \rightarrow 0$  with  $\mathcal{P}$ , and it can be shown that  $|h'(r_i)|/h(r_i) = O(\frac{1}{r_i})$ ,

$h(2 - r_i)/h(r_i) = O(r_i^n)$ ,  $b(r_i) = O[r_i^n(r_i - d_0)]$ ,  $P_{T,1}(r_1, P_{tot,2})/P_{T,2}(r_2, P_{tot,1}) = O[(\frac{r_1}{r_2})^n]$ , and  $\frac{\xi_0 \sigma^2 / h(r_1)}{P_{T,2}(r_2, P_{tot,1})} = O[(\frac{r_1}{r_2})^n]$ . Substituting into (37), it can be shown that the three terms on the right-hand side of (37) are  $O[r_1^{n-1}(r_2 - d_0)]$ ,  $O[r_1^{2n}(r_2 - d_0)^2/r_2]$ , and  $O[r_1^{2n}(r_2 - d_0)]$ , respectively. Since  $r_i \ll 1$  and  $(r_2 - d_0)/r_2 < 1$ , the first term dominates for small enough  $\mathcal{P}$ . This term is strictly negative, hence Theorem 3 is valid for the (IL,PL) segment of  $\bar{\mathcal{Q}}$ . A similar argument shows that Theorem 3 is valid for the (PL,IL) segment. Furthermore, the condition on the derivatives of the segments at the intersection point stated in Theorem 2 implies that the intersection of the regions defined by the two boundary segments is convex. Taking the intersection of this region with the code/demand rectangle gives a convex feasible region, which completes the proof of Theorem 3.

To prove Theorem 4, we solve for  $P_{tot,i}$  in (15) and (17), i.e.,

$$\frac{P_{tot,i}}{\sigma^2} = \frac{c_i a(r_i) + c_i b(r_i) c_j a(r_j)}{1 - c_i b(r_i) c_j b(r_j)}. \quad (38)$$

Along the power curve, as  $\mathcal{P} \rightarrow \infty$ , we have  $P_{tot,i} \rightarrow \infty$  for at least one  $i$ . It follows that

$$c_1 b(r_1) c_2 b(r_2) \rightarrow 1 \quad (39)$$

Because  $b(\cdot)$  is bounded and differentiable, we can take the derivative of (39) with respect to  $r_1$  to show that as  $\mathcal{P} \rightarrow \infty$ ,

$$\frac{dr_2}{dr_1} \rightarrow -\frac{\frac{h(r_2)}{h(2-r_2)} b(r_2)}{\frac{h(r_1)}{h(2-r_1)} b(r_1)} \quad (40)$$

If  $\frac{h(r')}{h(2-r')} b(r')$  is increasing with  $r'$ , then as  $r_1$  increases and  $r_2$  decreases,  $|dr_2/dr_1|$  decreases. Hence for large enough  $\mathcal{P}$ , the two power curve segments in Theorem 2 must be convex.

## B Expressions for Shadow Costs

Here we give expressions for the shadow costs that satisfy (27)-(28), assuming  $L_1 \leq L_2$ . We consider different cases corresponding to the different possible sets of binding constraints at the optimal allocation.

If the cells at the optimum allocation are (D/CL, D/CL), then

$$\lambda_{c,i} = u_0, \quad \lambda_{p,i} = 0, \quad (i = 1, 2) \quad (41)$$

This case is illustrated in Figure 3. The utility can be increased only by increasing the cell radius (if DL) or the number of codes (if CL).

If the cells are (PL, PL), then

$$\lambda_{c,i} = 0, \quad \lambda_{p,i} = u_0 \left( \frac{1}{P_{T,i}(r_i, P_{tot,j})} - \frac{c_j b(r_j)}{P_{T,j}(r_j, P_{tot,i})} \right), \quad (i = 1, 2 \text{ and } i \neq j) \quad (42)$$

This case is illustrated in Figure 4(a). The utility can be increased only by increasing the power limit. It can be shown from these expressions that  $\left. \frac{dr_2}{dr_1} \right|_{PL-} > -L_1/L_2 > \left. \frac{dr_2}{dr_1} \right|_{PL+}$ , and hence the (PL,PL) point intersects a line with slope  $-L_1/L_2$ .

If cell  $i$  is PL and cell  $j$  is D/CL, then

$$\begin{aligned} \lambda_{c,i} &= 0, & \lambda_{p,i} &= u_0 \left( \frac{1 - c_i c_j b(r_i) b(r_j)}{P_{T,i}(r_i, P_{tot,j})} \right) \\ \lambda_{c,j} &= u_0 \left( 1 - \frac{c_i b(r_i) P_{T,j}(r_j, P_{tot,i})}{P_{T,i}(r_i, P_{tot,j})} \right), & \lambda_{p,j} &= 0 \end{aligned} \quad (43)$$

This case is illustrated in Figure 4(b) (for (PL, D/CL)) and Figure 4(c) (for (D/CL, PL)). At the optimal point  $\left. \frac{dr_2}{dr_1} \right|_+ < -L_1/L_2$  and  $\left. \frac{dr_2}{dr_1} \right|_- = 0$ .

If the cells are (IL, PL), then

$$\begin{aligned} \lambda_{c,1} &= 0, & \lambda_{p,1} &= 0 \\ \lambda_{c,2} &= 0, & \lambda_{p,2} &= u_0 \left( \frac{1}{P_{T,2}(r_2, P_{tot,1})} - \frac{c_1 b(r_1)}{P_{T,1}(r_1, P_{tot,2})} \right) \end{aligned} \quad (44)$$

This case is illustrated in Figure 5(a). At the optimal point  $\frac{dr_2}{dr_1} = -L_1/L_2$ .

If the cell phases at the optimum are (IL, PL+D/CL), then

$$\begin{aligned} \lambda_{c,1} &= 0, & \lambda_{p,1} &= 0 \\ \lambda_{c,2} &= u_0 \left( 1 - \frac{P_{T,2}(r_2, P_{tot,1})}{c_2 b(r_2) P_{T,1}(r_1, P_{tot,2})} \right), & \lambda_{p,2} &= \frac{u_0}{P_{T,1}(r_1, P_{tot,2})} \left( \frac{1}{c_2 b(r_2)} - c_1 b(r_1) \right) \end{aligned} \quad (45)$$

This case is illustrated in Figures 5(b-c). Here both the code/radius and power constraints are binding in cell 2. At the optimal point  $\left. \frac{dr_2}{dr_1} \right|_+ < -L_1/L_2$  and  $\left. \frac{dr_2}{dr_1} \right|_- = 0$ .

## References

- [1] J. K. MacKie-Mason and H. R. Varian, "Pricing congestible network resources", in *IEEE Journal on Selected Areas in Communications*, Vol. 13, No. 7, September 1995.

- [2] R. Cocchi, S. Shenker, and L. Zhang, "Pricing in computer networks: motivation, formulation, and example", in *IEEE/ACM Transactions on Networking*, Vol. 1, No. 6, December 1993.
- [3] S. Jordan and H. Jiang, "Connection establishment in high-speed networks", in *IEEE Journal on Selected Areas in Communications*, Vol. 13, No. 7, September 1995.
- [4] F. P. Kelly, A. K. Maulloo, and D. K. H. Tan, "Rate control for communication networks: shadow prices, proportional fairness, and stability", in *Journal of the Operational Research Society*, Vol. 49, pp. 237-252, 1998.
- [5] C. U. Saraydar, N. B. Mandayam, and D. J. Goodman, "Pricing and power control in a multicell wireless data network", in *IEEE Journal on Selected Areas in Communications*, 19(10):1883-1892, October 2001.
- [6] L. Song and N. B. Mandayam, "Hierarchical SIR and rate control on the forward link for CDMA data users under delay and error constraints", in *IEEE Journal on Selected Areas in Communications*, 19(10):1871-1882, October 2001.
- [7] Y. Lu and R. W. Broderon, "Integrating power control, error correction capability, and scheduling for a CDMA downlink system", in *IEEE Journal on Selected Areas in Communications*, 17(5):978-989, May 1999.
- [8] D. J. Goodman and N. B. Mandayam, "Power control for wireless data", in *IEEE Personal Communication Magazine*, 7:48-54, April 2000.
- [9] D. Famolari, N. Mandayam, and D. J. Goodman, "A new framework for power control in wireless data networks: games, utility, and pricing", in *Wireless Multimedia Network Technologies*, pp. 289-310, 1999.
- [10] H. Ji and D. Huang, "Non-cooperative uplink power control in cellular radio systems", in *Wireless Networks*, (4): 233-240, 1998.
- [11] P. Liu, M. Honig, and S. Jordan, "Forward link CDMA resource allocation based on pricing", in *Proc. IEEE WCNC 2000*, September 2000.

- [12] P. Liu, P. Zhang, S. Jordan, and M. Honig, “Single-cell forward link power allocation using pricing in wireless networks”, to appear in *IEEE Transactions on Wireless Communications*.
- [13] P. Marbach and R. Berry, “Downlink resource allocation and pricing for wireless networks”, in *Proc. Infocom 2001*, New York City.
- [14] C. D. Frank and E. Visotsky, “Adaptive Interference Suppression for CDMA with Long Spreading Codes”, in *Proceedings Allerton Conference on Communications, Control, and Computing*, September 1998.
- [15] C. Zhou, M. L. Honig, and S. Jordan, “Two-Cell Power Allocation for Wireless Data Based on Pricing”, in *Proc. Allerton Conference on Communications, Control, and Computing*, Monticello, IL, Oct. 2001.
- [16] R. K. Sundaram, *A First Course in Optimization Theory*. New York: Cambridge University Press, 1996.
- [17] H. R. Varian, *Microeconomics Analysis*, 3rd ed., W. Norton and Company, Inc., 1992.
- [18] C. Zhou, M. L. Honig, S. Jordan, and R. Berry, “Forward-Link Resource Allocation for a Two-Cell Voice Network with Multiple Service Classes”, in *Proc. Wireless Communications and Networking Conference*, New Orleans, La., March 2003.

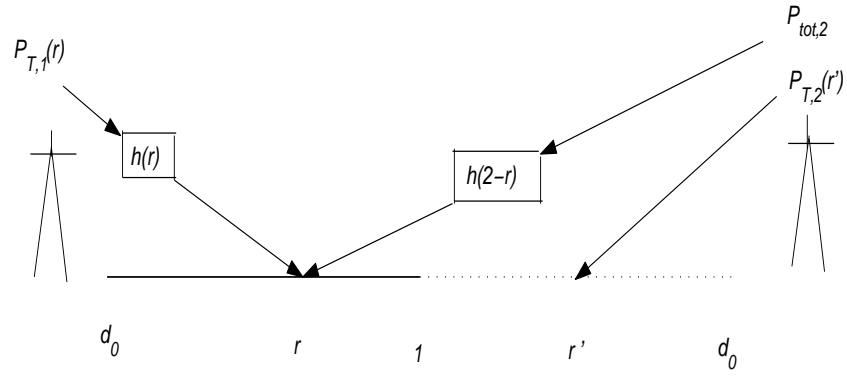


Figure 1: One-dimensional, two-cell model.

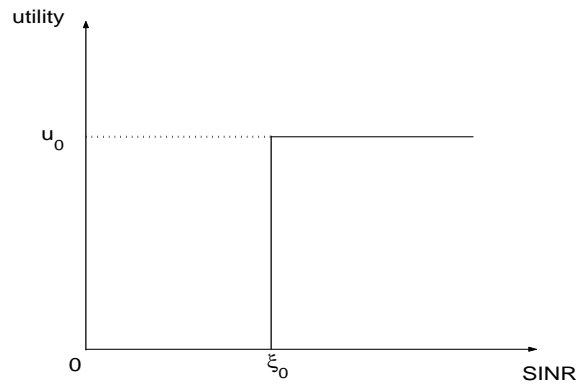


Figure 2: Utility function for a fixed-rate (voice) service.

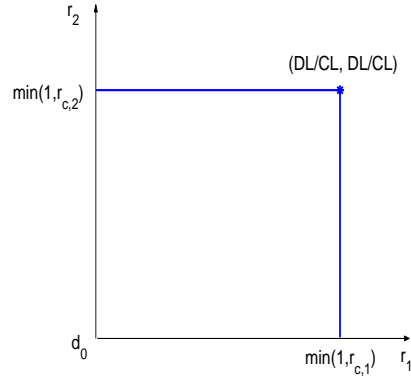


Figure 3: A feasible region in the class  $\mathcal{T}_1$ .

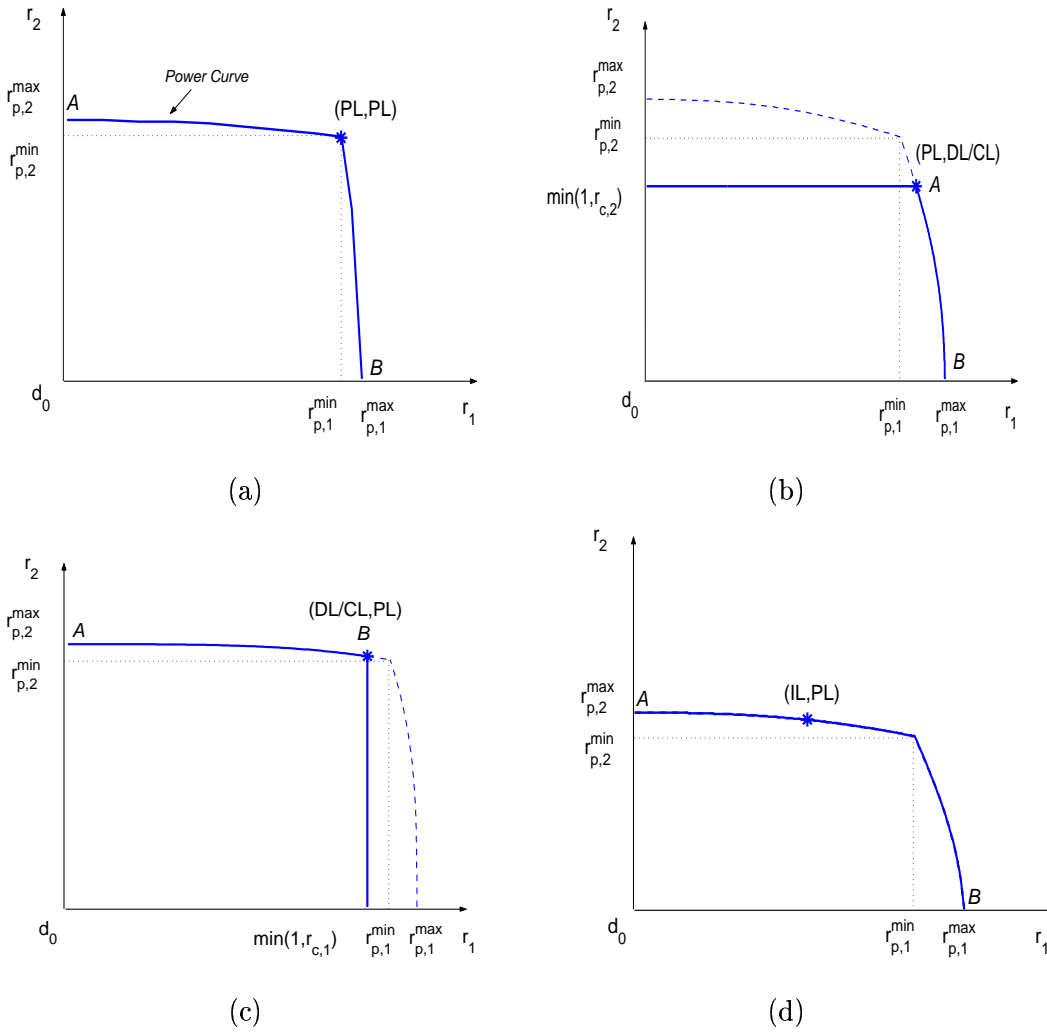


Figure 4: Examples of feasible regions in the class  $\mathcal{T}_2$ .

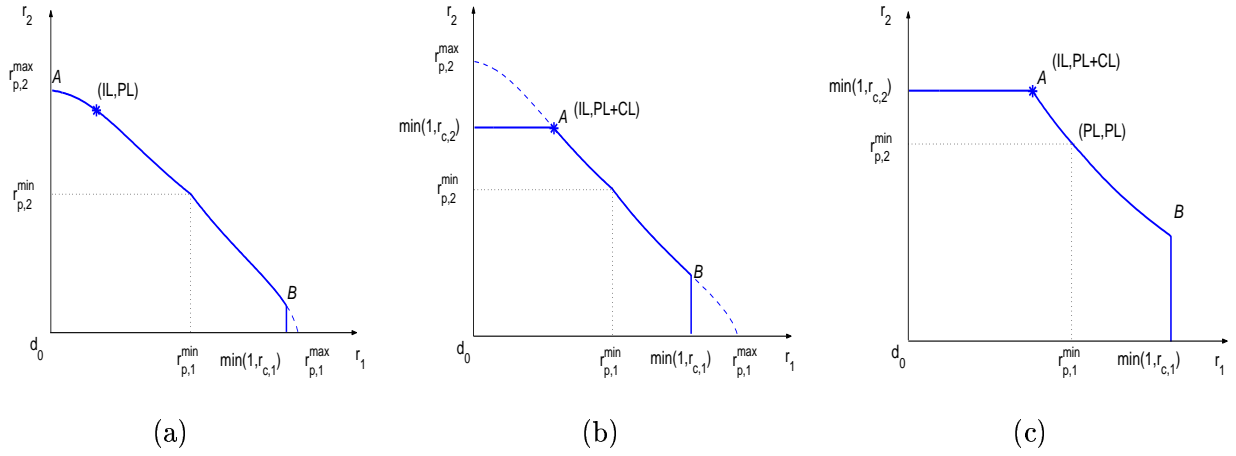


Figure 5: Examples of feasible regions in the class  $\mathcal{T}_3$ . The power curves in (a) and (b) are neither convex nor concave, whereas the power curve in (c) is convex.

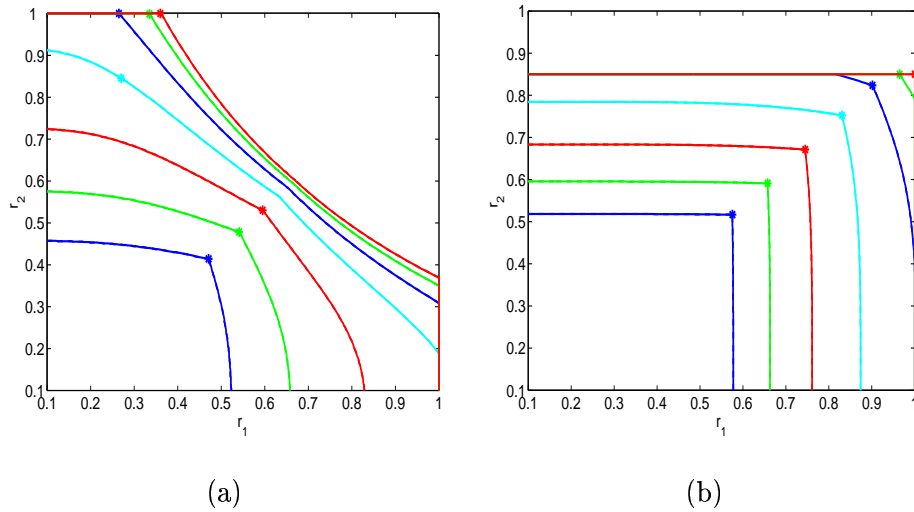


Figure 6: Boundary of  $\mathcal{R}$  for different values of  $\mathcal{P}$ . The asterisks correspond to the maximum value of  $L_1 r_1 + L_2 r_2$ . (a)  $\frac{\mathcal{P}}{\sigma^2} = 20, 23, 26, 29, 32, 35$  and  $38$  dB; (b)  $\frac{\mathcal{P}}{\sigma^2} = 30, 33, 36, 39, 42, 45,$  and  $48$  dB.

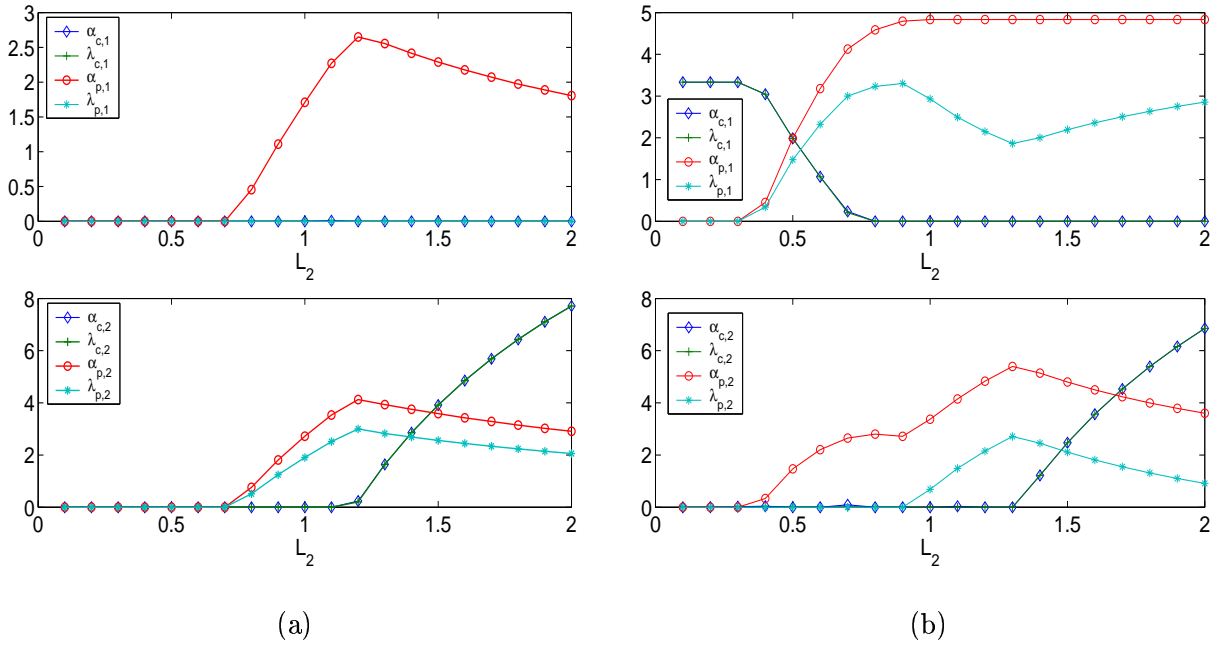


Figure 7: Optimal prices and shadow costs associated with resource constraints versus the load in cell 2: (a)  $L_1 = 0.7$ ,  $\frac{P}{\sigma^2} = 23$  dB; (b)  $L_1 = 1.2$ ,  $\frac{P}{\sigma^2} = 23$  dB.